Theoretical Validation of Experimentally Determined Beam Quality Correction Factors For the 6 MeV and 6 MV Linear Accelerator Radiotherapy Beams At University of Nigeria Teaching Hospital, Ituku-Ozalla, Enugu State In South Eastern Nigeria

Owojori A. A. and Okunnade A.A

Department of Physics and Engineering Physics, Obafemi Awolowo University, Ile-Ife, Nigeria

(Received January 27, 2020; Revised March 14, 2020; Accepted May 28, 2020)

Abstract

Experimental Beam quality correction factors, kQ, for three ion chambers (ICs) have been validated for linear accelerator (LINAC) beams used for a calibration process at the University of Nigeria Teaching Hospital (UNTH) facility in Nigeria. The beam transport processes within the LINAC treatment head were simulated with the BEAMnrc Monte Carlo (M.C.) package of EGSnrc suite, while the beam transport processes within the Phantom-IC geometries were simulated with the DOSXYZnrc Monte Carlo (M.C.) package of EGSnrc suite. The computation of the kQ values were obtained from depth-dose distributions generated from DOSXYZnrc. The kQ calculated for the three ion chambers (ICs) –Farmer IC, Semi-Flex IC and Advanced Markus IC – are in good agreement with the experimentally determined kQ values. The values of calculated kQ for the Farmer IC deviated from the experimental kQ by 0.1%, while the Semi-Flex IC deviated by 0.9%. Calculated kQ value for the Advanced-Markus IC also deviated from experiment by 0.7%. The study concluded that MC.-determined beam quality correction factors, kQ, obtained using BEAMnrc and DOSXYZnrc packages can be used to validate experimental beam quality correction factor values for medical LINAC beams once geometric specifications and dimensions of calibration systems, alongside recommended dosimetry protocols have been incorporated.

Keywords: Monte Carlo, Beam quality correction factor, Phase space, depth ionization

1.0 Introduction

Accurate dose delivery is one of the benefits one gains when using the LINAC radiotherapy machine in treating superficial and deep-seated cancer. Calibration of the LINAC radiotherapy beams with respect to the ion chambers (ICs) used in a healthcare facility is necessary to maintain optimized dose delivery, most importantly after repairs or after prolong use. Reference dosimetry protocols, such as the International Atomic Energy Agency Technical Report Series 398 (IAEA TRS-398) [1] protocol forphoton beams, and the American Association of Physicists in Medicine Task Group 51 (AAPM TG-51) [2] protocols for electron beams, have become the most popular protocols for such calibrations today. The calibration techniques can be purely experimental or computational depending of the healthcare capabilities. The experimental calibration method involves determining the absorbed dose delivered to water at a reference depth in water for a LINAC photon or electron beam over the machine time (otherwise referred to as monitor unit (MU)). The calibration is used to standardize the dose delivered after certain successive monitor units. This calibration requires carrying the IC systems to a secondary of tertiary standards laboratory to standardize the beams with a reference Co-60 beam system, which can be very time consuming. The computational method, however, is less complicated - in that, treatment-head systems and IC systems geometries necessary for the calibration, and the transport of the LINAC beams within the geometries are simulated alongside. The calibrations can be done in-house at

* Corresponding author email: fope2010@gmail.com

ABC Publications Incorporated

the healthcare facility.

In this study, the LINAC's beam quality correction factors (kQ and kq,E) used in LINAC beam calibration were determined using computational simulation for three ICs resident at the university of Nigeria teaching hospital (UNTH).

2.0 Materials and Methods

2.1. Formalism for Beam Quality Correction Factor (kQ or kq,E) Determination

In this work, Two LINAC beams used in the experimental calibration method were simulated to project through a treatment head geometry of a LINAC machine, water phantom geometry and (ion chambers) ICs' sensitive volume geometries. The BEAMnrc code simulated the transport processes within the LINAC treatment head geometry and the DOSXYZnrc code simulated the transport processes within the water phantom geometry and ICs' sensitive volume geometry. The beam quality correction factors were determined from the depth-dose distributions plots. These simulated beam quality correction factors (kQsim and kq,Esim) were then compared with the experimental ones for the three ICs.

2.1.1 Formalism for Experimental Beam Quality Correction Factor (kQ or kq,E) Determination

The experimental calibration setup for the photon beam transport is shown in Figures 1 while the calibration setup for the electron beam transport is shown in Figure 2. As shown in Figure 1a, for the photon mode, an MV photon beam is generated as soon as the electron beam produced in the LINAC machine is sent into the heavy X-ray target material and then shaped by collimators into the water phantom material. The resulting accumulated ionizations produced in the phantom are eventually measured with ICs. In Figure 1b, a similar process occurs in the electron mode whereby the LINAC's electron

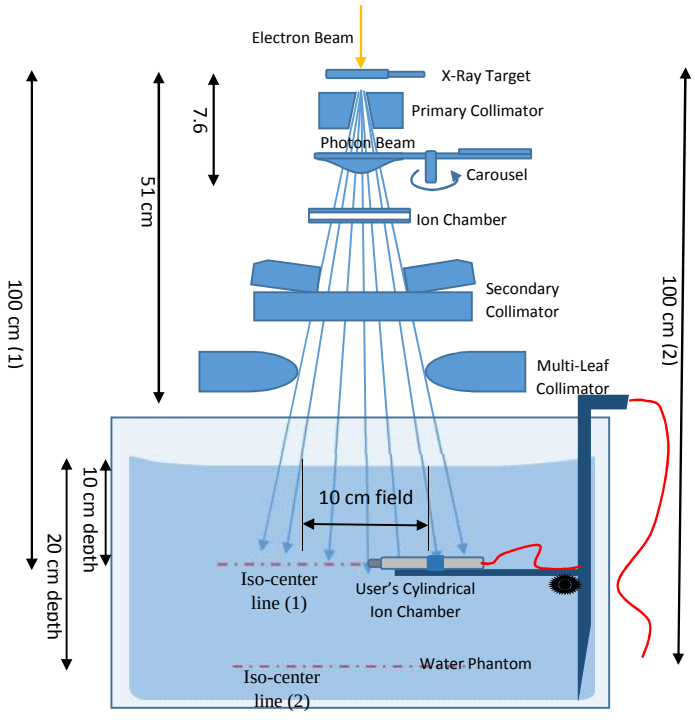

Figure 1a: LINAC beam calibration setup for photon beam mode based on $TPR_{20,10}$ index, which depend on the two iso-center lines (1) and (2)

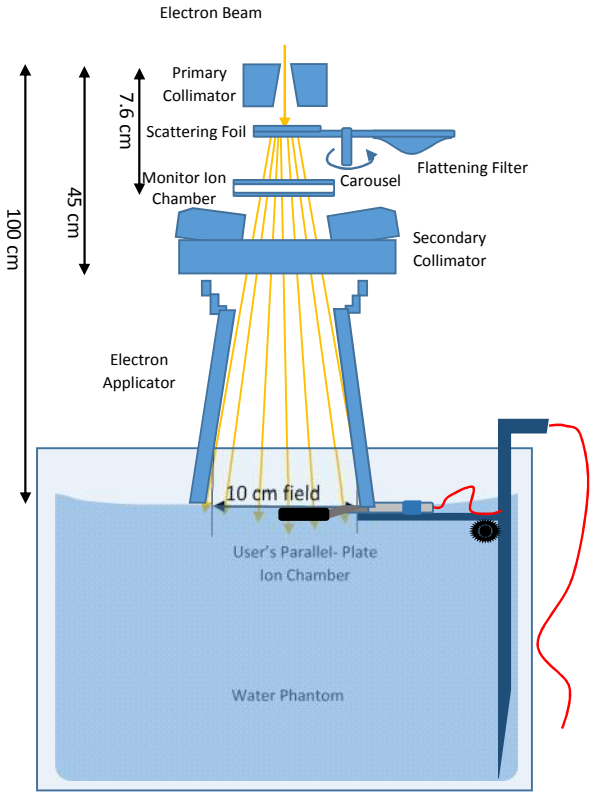

Figure 1b: LINAC beam calibration setup for Electron beam mode

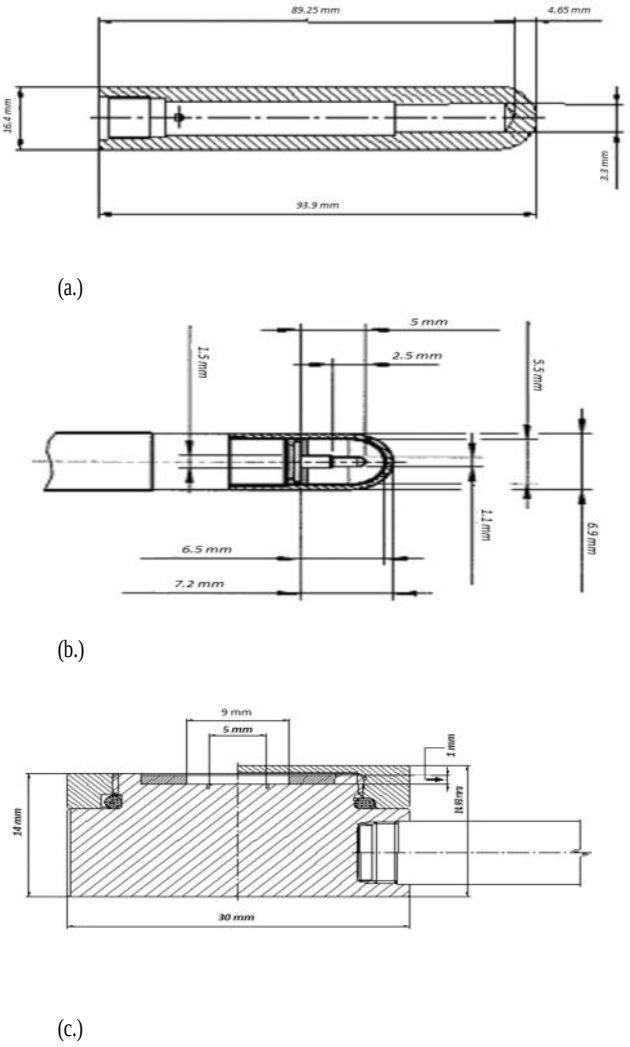

Figure 2: The User Ion Chambers at the Radiotherapy Facility (a.) the PTW 30013 Farmer IC (b.) the PTW 31010 Semi-Flex IC and (c.) the PTW-34045 Advanced Markus IC with geometrical dimensions in mm

beam is only collimated into the water phantom and the resulting ionizations are measured with ICs.

The computational approach involves simulating the electron or photon beam transport right through the LINAC's treatment head down to the phantom-IC setup and consequently taking desired measurements of the absorbed dose at protocol-specific recommended depths within the phantom system. The ionization occurring at specific depths in the water phantom are converted to depth-doses. Successive measurements results in absorbed doses per depth curve or depth-dose distribution curve which can be used to determine the beam quality correction factor for any specified photon beam quality, Q (or electron beam quality, [*q*,*E*]) delivered from the LINAC treatment head.

The beam quality correction factor (k_Q) is a correction for the radiation beam quality other than the beam, Q_0, used in its calibration when it is commissioned. The same k_Q factor is the parameter an experimenter ultimately determines to complete an experimental LINAC beam calibration. It is often assigned to each of the users' IC by the standard dosimetry laboratories. The standard dosimetry laboratories use Co-60 as the reference beam although some Primary Standards Dosimetry Laboratories (PSDLs) directly use photon and electron beams, depending on the availability within their laboratory.

The beam quality correction factor, k_Q can be written in terms of the calibration factors based on the reference beam, N_{D,w,Q_0} , the LINAC beam, $N_{D,w,Q}$

$$k_{Q,Q_0} = \frac{N_{D,w,Q}}{N_{D,w,Q_0}} \tag{2.3}$$

The absorbed dose to water, $D_{w,Q}$, at the users beam quality, Q, is given as:

$$D_{w,Q} = M_Q \quad N_{D,w,Q_0} \quad k_{Q,Q_0} \tag{2.4}$$

In which case, k_{QQ_0} can be restated as

$$k_{Q,Q_0} = \frac{D_{w,Q} / M_Q}{D_{w,Q_0} / M_{Q_0}} \tag{2.5}$$

With which the parameter D_{w,Q_0} is expressed as

$$D_{w,Q_0} = M_{Q_0} \quad N_{D,w,Q_0} \quad k_{Q_0,Q_0} \tag{2.6}$$

Under Co-60 beam, k_{QQ_0} has the value of unity.

However, the k_{QQ_0} has to be derived for each chamber used under users photon or electron beam quality.

2.1.2 Formalism for the Theoretical Beam Quality Correction Factor Determination

Theoretically, the k_{QQ_0} has been given by the expression [3], [4]:

$$k_{Q,Q0} = \frac{(s_{w,air})_Q \ P_Q \ W_{air,Q}}{(s_{w,air})_{Q0} \ P_{Q0} \ W_{air,Q0}} \quad (2.7)$$

where Q is a photon beam quality,
Q0 = Co-60 beam, PQ and
PQ0 are perturbation corrections for the ion chamber used in the beam qualities Q and Q0 respectively.

W_{air} is the mean energy required to create an ion pair.

For both beam qualities [5],

$W_{air,\ Q} = W_{air,\ Q0} = 33.94$ J/C (2.8)

Theoretical means of estimating $k_{Q,Q_0}s$ have been conducted in literature. Andreo [3] performed theoretical calculations on $k_{Q,Q_0}s$ for a series of user photon beam qualities, Q, based on their quality index, $TPR_{20,10}$. Sempau et al. [6] derived the $k_{Q,Q_0}s$ values from Monte Carlo Simulations of Ion chambers. Similarly, Wulff et al. [7] performed Monte Carlo calculations of $k_{Q,Q_0}s$ for photon beams based on perturbation factors influencing the users' cylindrical ICs and discovered that some factors from constructive details of the ICs show no influence on its k_{Q,Q_0}

Recent studies by [8] on the k_{Q,Q_0} has shown that it is better to determine the values of k_{Q,Q_0} for the users' ICs other than the reference ICs in the users beam quality, based on their quality indexes.(R50 and TPR20,10). The estimation of $k_{Q,Q_0}s$ based on the influence of perturbation factors in parallel plate ICs under electron beams have been researched on most recently by Zink and Wulff [9]. Their findings show that the wall correction factor, which has been assumed negligible, was in fact, not dependent on the user beam quality index derived from Monte Carlo simulations.

2.2. Theoretical Calibration Setup and Procedure

In this work, the absorbed dose at specified depths due to a beam quality (Q or q,E) was determine theoretically. The experimental calibration procedure was simulated using the IAEA TRS-398 and AAPM TG-51 dosimetry protocol guide adopted in the experimental LINAC beam calibration at the UNTH facility. The IAEA TRS-398 protocol guide was used for photon beam dosimetry while the AAPM TG-51 protocol guide was used for electron beam dosimetry. The absorbed dose was experimentally determined using an IC to measure ionizations created due to the LINAC beam impinged on a phantom medium. A typical LINAC beam calibration setup for photon beam and electron beam mode are as shown in Figures 1a and 1b respectively. This LINAC beam calibration setup and procedure was simulated using the BEAMnrc and DOSXYZnrc package. The BEAMnrc code simulates the photon and electron beam transports from the treatment head units down to the phantom surface and a phase space data was collected. The DOSXYZnrc code on the other hand simulates the photon and electron beam transport within the phantom-IC system and generates the dose distribution collected in the sensitive region of the ICs. The Monte Carlo algorithm incorporated in the package simulates the random nature of the beam transport within the Co-60 and LINAC treatment head, and the phantom-IC setup.

The first step is to collect the LINAC and Reference beam (Co-60) treatment head geometry details, calibration factors, ion chamber and phantom geometry details.

The second step is to set up the material specifications, dimensions and positions of the beam source and treatment-head systems as described experimentally, in the BEAMnrc code.

The third step is to run the BEAMnrc code and collect the phase space data collected at the outlet channel side of the simulated treatment head units. The BEAM data processor (BEAMdp) is used to process the phase space data.

The fourth step is to set up the material specifications, dimensions and positions of the distributed beam sources (from processed phase space data) and phantom-IC systems, as described experimentally, in the DOSXYZnrc code.

The fifth step involves running the DOSXYZnrc code and generating accumulated ioni-

zations per depth (or depth-ionization distribution) in the sensitive region within ion chamber for every phantom-IC simulation. These ionizations per depth are converted to depth-dose distributions with the DOSXYZnrc code and are presented in *.3ddose extension files. Depth dose data can then be represented on a 2D plotting program such as Microsoft Excel. The k_Q values based on beam quality index (TPR20,10 for photon beams or R_{50} for electron beams) can then be derived from the depth-ionization or depth-dose distribution curves.

Table 1: Ionization Chamber Specifications used in this work ***(****source: PTW-Freiburg [11])*

Type No.	***Chamber Name***	***Measuring Volume (cm^3)***	***Entrance Window***	***Electrode Diameter (mm)***	***Window Area Density (mg/cm^2)***	***Electrode Distance (mm)***	***Ion Collection Time at nominal HV***
PTW 30010	Farmer	0.6	0.335 mm PMMA + 0.09 mm C	Aluminium (Al)- 1.1 mm	57 Graphite Density (1.85 g/cm^3)	3.05	0.14 ms (400 V)
PTW 30013	Semi-Flex	0.125	0.55 mm PMMA + 0.15 mm C	Aluminium (Al) - 1.1 mm	78 Graphite Density (0.82 g/cm^3)	2.75	Ms (400 V)
PTW 34045	Advanced Markus	0.02	0.87 mm PMMA + 0.4 mm Air + 0.03 mm CH_2 (Polyethylene) [with protection cap in place]	5	106	1	0.02 ms (300 V)

C – Carbon, Al –Aluminum, CH_2 – Methyl-, PMMA – Acrylic, HV – High Voltage

The Elekta Precise LINAC treatment head model is the photon and electron beam output channel unit at the university of Nigeria teaching hospital (UNTH) healthcare facility in Enugu, while the Theratron-780 Cobalt-60 treatment head model is the reference Co-60 beam output channel at the tertiary standards laboratory in the University College Hospital (UCH), Ibadan.

Also, three IC model have been used for the purpose of the LINAC beam calibration. A reference Farmer IC (PTW 30013) and a Semi-Flex IC (PTW 31010) have been used for the calculation of the absorbed dose due to photon beams while an Advanced Markus IC (PTW 34045) have been used for the calculation of the absorbed dose due to electron beams. Geometric details of the ICs have been presented in Figure 2 and the individual IC specifications have been tabulated in Table 1. A water phantom with known dimensions was used as it closely approximates the radiation absorption and scattering properties of soft tissues, alongside its availability [10]. With appropriate dosimetry protocol using the two recommended booklets (IAEA TRS-398 and AAPM TG-51) determine the LINAC beam calibration setup for both electron beam mode and photon beam mode.

2.2.1 Simulating the Treatment Head Setup with BEAMnrc Package on Workstation Personal Computer

With the HP™ high-performance workstation personal computer (PC) of the theoretical physics laboratory of the department of Physics and Engineering Physics in the Obafemi Awolowo University (OAU), the BEAMnrc package was initialized and the parameter values of the Cobalt-60 and LINAC accelerator treatment head components were inputted. Appropriate cross section data types were either selected or created and the input parameters of the accelerators were activated. The prepared input file which contains the input parameter values and instructions was loaded into BEAMnrc to provide the input parameters and run the transport process for beams in the system. A minimum of 1 x 108 particle histories were sampled for each Co-60 and

LINAC treatment head transport simulation. The Theratron-780 Co-60 machine treatment and Elekta Precise Treatment head units were both simulated in the BEAMnrc package. All experimental reference conditions were used in the simulation to mimic the systems as much as possible. In the Co-60 treatment head setup, a Co-60 beam was simulated while in the LINAC treatment head setup, 6 MeV electron beam and 6 MV photon beam were simulated across the treatment head geometries. Results of the beam transport in the treatment head geometries were collected in a phase space data file and were analyzed with the BEAM data processor (BEAMDP) for fluence distribution variations [12].

2.2.2 Simulating the Water Phantom-Ion Chamber Setup with DOSXYZnrc Package on Workstation Personal Computer

The phase space data file which contains the emergent particles' details from the treatment head simulation is fed as input distributed source file for the water phantom - ion chamber setup simulation using in the DOSXYZnrc package, a dose- simulation and analysis package of the EGSnrc software suite. In DOSXYZnrc, the water phantom and ion chamber geometries are subdivided into voxels, each with dimensions of about 0.02cm length, 0.02cm breath and 0.02cm width. After a complete run, a *.3ddose file, which contain the depth- ionization distributions (DIDs) data within the air cavities of each of the ion chambers was obtained, and presented with another package under the EGSnrc suite called STATDOSE which deliver a 2D output of dose profiles like the central-axis depth-dose profiles and lateral dose profiles were obtained according to appropriate formalisms prescribed for central-axis depth dose calculations. The appropriate beam quality indices (TPR20,10 and R50) were obtained from the depth-dose profiles.

2.2.3 Estimation of Absorbed Dose and calculation of Beam Qualities

The relative depth-ionization distributions plot with depths for both photon and electron beam calibrations and the depth-dose ionization curves were used to obtain the photon and electron beam quality indices, $TPR_{20,10}$ and R50, respectively. The $TPR_{20,10}$ (in the case of the photon beams) was obtained from the relative ionization distribution (which alternatively represents the relative distributions of absorbed dose). This was done by calculating the percent-depth dose ($PDD_{20,10}$) at depth 20 cm and 10 cm of the depth ionization distribution for my depth-dose curves, the $TPR_{20,10}$ was then derived by the equation

$$TPR_{20,10} = 1.2661\, PDD_{20,10} - 0.0595 \qquad (2.9)$$

the $TPR_{20,10}$ index was used to look up the available dosimetry data to obtain the k_{Qs} for the ICs whose k_Q data have been presented. Also the measured depth ionization distribution of the simulated calibrated beam (in the case of the electron beams) was used to calculate the half-value ionization depth, $R_{50,ion}$, which was used to obtain the electron beam quality index (R_{50}). A simple relation between $R_{50,ion}$ and R_{50} for $R_{50,ion}$ depths less than or equal to 10 g/cm2 is given as

$$R_{50} = 1.029\, R_{50,ion} - 0.06 \quad (g/cm^2) \qquad (2.10)$$

Tables of the electron beam quality correction factor ($k_{q,E}$) as a function of R_{50} for the user's electron ionization measuring IC were look up in the dosimetry booklet [1]. The simulated beam quality correction factors (k_{Qsim}, $k_{q,Esim}$) were then compared with the experimental (k_{Qexp}, $k_{q,Eexp}$). The electron depth-ionization distribution were also multiplied with their stopping power ratios ($s_{w,air}$) [13] at each depth to convert to doses at such depth in the case of electron beam simulation and Co-60 beam (with a constant $s_{w,air}$ = 1.133 at all depths ([1])

The relation between the chamber-cavity absorbed dose ($D_{chamber}$) and the absorbed dose to water (D_w) for respective ICs was thus given as

$$D_w = D_{chamber} \quad P_Q \quad s_{w,air} \qquad (2.11)$$

where, PQ , the perturbation correction unique to each IC in particular beam quality,

Q, was estimated from already established tables in literature [11]

2.2.4 Beam Quality Correction Factors (kQ) Calculation

Adopting the formalism in equation (2.11) for an ideal ion chamber measuring the absorbed dose-to-water, the relation can be elaborated for an actual ion chamber type due to the influence of a LINAC beam quality, Q as

$$D_{w,Q} = D_{air,Q}\ P_Q\ (s_{w,air})_Q \tag{2.12}$$

where PQ can be evaluated for the ICs using the PTW brochure [11] *and* $(s_{w,air})_Q$ *can be calculated at any reference depth using the equations prescribed in the IAEA Code of Practice booklet.*

The $D_{air,Q}$ calculated above was used to calculate k_{Q,Q_o} theoretically for photon and electron beams appropriately.

$D_{w,Q}$ was derived directly from the depth ionization distribution derived from simulation using the conditions provided by IAEA code of practice [1] for absorbed dose calculation from the central axis due to photon and electron beams.

2.2.4.a kQ for Photon Beams

i. Ratio Approach used in MC. Simulation:

The beam-dependent beam-quality correction factor, as prescribed in the IAEA TRS 398, was related to the perturbation factors unique to the respective ICs, P_Q. With the relation between stopping power ratios and water-cavity dose ratio

$$(s_{w,air})_Q \cdot P_Q = \frac{D_w}{D_{air}} \tag{2.13}$$

$k_{Q,Qo}$ was, according to the works of Sempau et al. [6] and Capote et al. [14], related as:

$$k_{Q,Q0} = \frac{\left[\dfrac{D_w}{D_{air}}\right]_Q}{\left[\dfrac{D_w}{D_{air}}\right]_{Q0}} \tag{2.14a}$$

Therefore, for every ion chamber present, this can be restated as

$$\left[k_{Q,Q0}\right]^{IC} = \left[\frac{\left[\dfrac{D_w}{D_{air}}\right]_Q}{\left[\dfrac{D_w}{D_{air}}\right]_{Q0}}\right]^{IC} \tag{2.14b}$$

Hence, this formalism was used in our calculation of $k_{Q,Qo}$ at reference point for the farmer reference ion chamber and Semi-Flex ICs.

The dimensions of the main material constituents of the ICs have been listed in Table 2.

2.2.4.b Kq,E for Electron Beams

i. The MC-Perturbation Combined Approach used in MC Simulation:

Using the relation of the beam quality correction factor as expressed in equation 2.7, and the assumption given in equation 2.8 the formalism given in DIN 6800-2 recast the expression to

$$\left[k_{Q,Q0}\right]^{IC} = \left[\frac{\left(s^{\Delta}_{w,air}\right)_Q}{\left(s^{\Delta}_{w,air}\right)_{Q0}}\ \frac{\left(p_{wall}\ \ p_{cav}\right)_Q}{\left(p_{wall}\ \ p_{cav}\right)_{Q0}}\right]^{IC} \tag{2.19}$$

where Δ is the 10 keV cut-off energy and $\left(s^{\Delta}_{w,air}\right)_{Q0}$ *is the water-to-air stopping power ratio for the reference beam, Q0, having a value 1.133.*

$\left(s^{\Delta}_{w,air}\right)_Q$ at zref can be calculated empirically from the expression given by the IAEA TRS-398 protocol

$$\left(s^{\Delta}_{w,air}\right)_Q(z_{ref}) = 1.253 - 0.1487\,(R_{50})^{0.214} \tag{2.20}$$

$(P_{wall})_{Qo}$ have been calculated for Co-60 [9] to have the value 1.0094

$$\left(p_{cav}\right)_Q = 1 - 0.037\ e^{-0.27 \cdot R_{50}} \tag{2.21}$$

$(P_{wall})_{Qo}$ as derived from interpolation of the graph results of Zink and Wulff [9] was of value 1.02

where Q_0= Co-60,

R_{50} was derived from the depth ionization distribution curve using its R50,ion value, expressed thus:

$$R_{50} = 1.029\,R_{50,ion} - 0.06\ \ g/cm^2 \tag{2.22}$$

Prior to Figure 2c, the IC window's geometrical thickness specification was corrected in simulation due to non-water-equivalence of the entrance windows of the Plane parallel ion chambers. The effective point of measurement was adopted in the simulation, in which the window's water-equivalent thickness (d_w in g/cm2) rather than the geometrical thickness, (d_P in g/cm2) was adopted. The geometrical and water equivalent thickness are related as [11].

$$d_w = d_p \frac{\rho_p}{\rho_w} \quad (2.23)$$

where P_P and Pw are the densities (in g/cm^3) of the entrance window and water respectively.

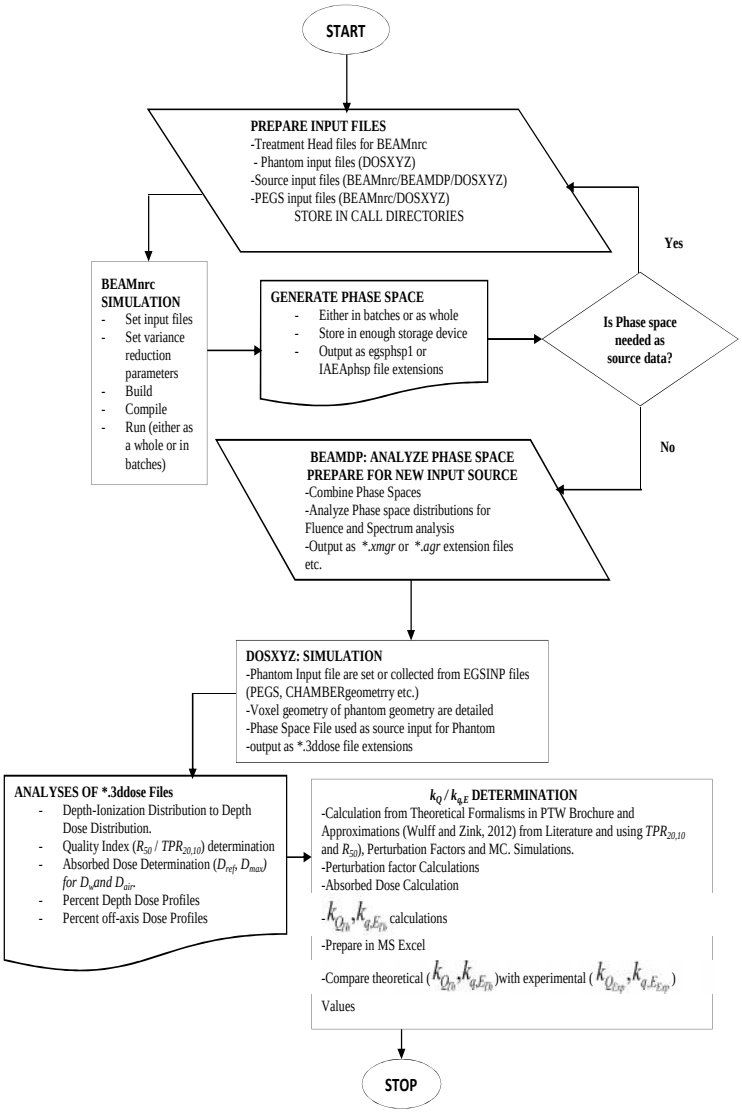

Figure 3: The Structure of the Computational Simulation

3. Results and Discussions

3.1 Phase Space Statistics Results from Simulation with BEAMnrc

The BEAMnrc preview display of the Co-60 gamma, 6 MV photon and 6 MeV electron beam treatment head generated for the simulations have been presented in Figures 4, 5 and 6 respectively. The sources to surface distance for the setup were 80 cm, 100 cm and 100 cm respectively as illustrated in Figures 4, 5 and 6. This was necessary for proper imitation of the treatment head setup in the experimental calibration.

A total of 29 gigabyte (GB) storage of phase space data have been generated from BEAMnrc package. This was necessary to gather enough particles sources for the phantom-chamber simulations. The larger the number of particles to run the Monte Carlo Simulation, the higher the approximations of the values to expected values. Five billion (5 x 109) gamma photon were sampled respectively within Co -60 treatment head while 1.7 million (1.7 x 108) X-ray photon and 1.8 million (1.8 x 108) electron particles were sampled respectively within the Elekta Precise treatment head.

3.1.1 Simulation of the Co-60, 6MV and 6 MeV Beam

The phase space particle statistics for each beam have been presented in Table 2. About 99 % of the generated particles from the Co-60 phase space file were gamma photon particles, 99 % of the generated particles were X-ray photon particles in the 6 MV phase space file and 99% of the generated particles were electron particles in the 6 MeV phase space file. This was important in ensuring minimal contamination of particles when interacting with the phantom medium.

3.1.2 BEAMDP Analysis of Co-60, 6 MV and 6 MeV Phase Space Distributions

The spectrum distribution for the treatment head results have been presented in Figures 7, 8, 9, 10 and 11. The central-axis energy spectrum for the Co-60 beam presented in Figure 5 shows the two prominent gamma photo-peaks (1.17 MeV and 1.33 MeV) of the Co-60 source as expected. The

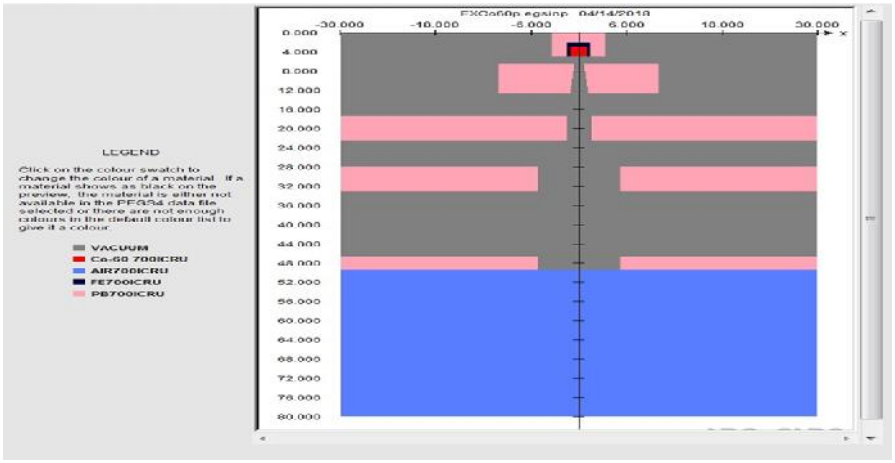

Figure 4: The Treatment Head Preview Generated from the Input Files Modified for Theratron-780 Co-60 Machine

Compton continuum observed from the left-hand side of the photo-peaks are as a result of scattering of the gamma photon on interacting with the primary and secondary collimators which generate small k-shell X-ray fluorescence peaks at keV energies.

The 6 MV central-axis energy distributions in Figure 6 show an X-ray energy peak of around the 0.4 MeV. This was the consequence of not using the accelerator beam energies as beam specifiers because the beam specification was not the true reflection of what is always obtained in terms of quality at the phantom-medium end. The quality index specifier was, therefore, more important in such a case. The electron energy peak of the 6 MV electron distributions had a maximum peak at 0.75 MeV as shown in Figure 7. The 6 MeV central axis energy distribution spectrums also show 2 electron-energy peaks around the 6 MeV region and very low photon energies as shown in Figure 8. The 6 MeV spectrum has two prominent electron peak distributions around 6.3 and 6.7 MeV energy as shown in Figure 9 while the photon spectral distributions as shown in Figure 10 had a maximum peak at about 0.1 MeV.

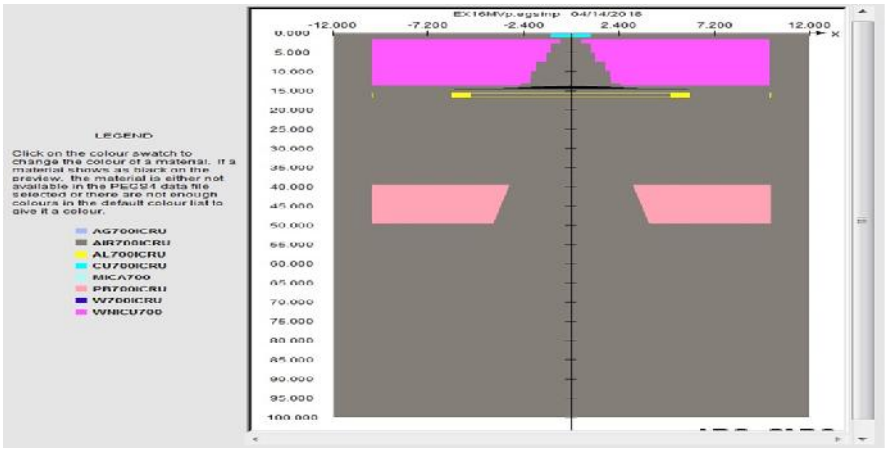

Figure 5: The Treatment Head Preview Generated from the Input Files Modified for Elekta Precise LINAC Machine in Electron-Therapy Mode

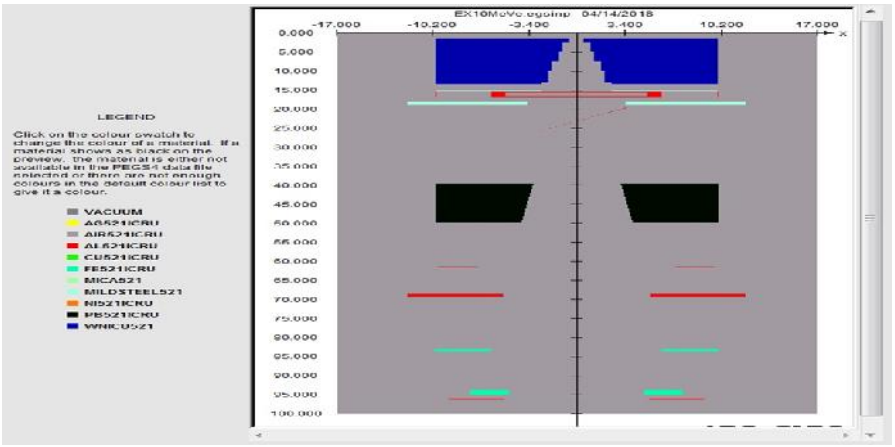

Figure 6: The Treatment Head Preview Generated from the Input Files Modified for Elekta Precise LINAC Machine in Electron-Therapy Mode

3.2 Beam Profiles

The important beam profiles presented were the depth-dose beam profile and the central axis lateral dose profiles for the Co-60, 6 MV and 6 MeV simulation carried out in this work. Comparisons of respective beam profiles were performed and reported.

3.2.1 Depth-Dose Profiles

The Percentage depth-dose profiles have been obtained for the Theratron 780 Co-60 beam, the Elekta Precise's 6 MV and 6 MeV beams. These profiles have been derived at reference

Table 2: Phase Space Statistics of Co-60, 6 MV and 6 MeV Beams

Type of Beam	*Number of incident Particles*	*Number of Particles in file after Simulation*	*Number of Photons*	*Number of Electrons / Positrons*	*Maximum Energy of the Particles (MeV)*
Theratron 780 - Co-60 beam					
Co-60	5 x 10^9	8940562	8883181	57381	1.744
6 MV Beam from the Elekta Precise LINAC Treatment Head					
Photon	1.7x 10^8	126491813	125806703	685110	5.823
6 MeV Beam from the Elekta Precise Treatment Head.					
Electron	1.8 x 10^8	379408977	377352250	2056727	5.897

conditions. In Figures 11 and 12, the sharp buildup effect of the absorbed dose was observed in the Co-60 gamma beam up to a maximum, at about 0.5 cm of depth, and then the dose falls off less rapidly with higher depth. The 6 MV X-ray beam in Figure 3.9 has its absorbed dose buildup from the skin surface of the phantom up to a maximum, at about 1.5 cm of depth, then falls off gradually. Also at about 10 cm, a depth expected to have a treatment target, the absorbed dose delivered at this depth for the Co-60 beam was only about 58% while the 6 MV beam was about 64 %.

Furthermore, absorbed dose from the Co-60 beam was not efficient enough in deep treatment compared with the 6 MV beam Also observed was that the Co-60 gamma beam deposits about 30 % of

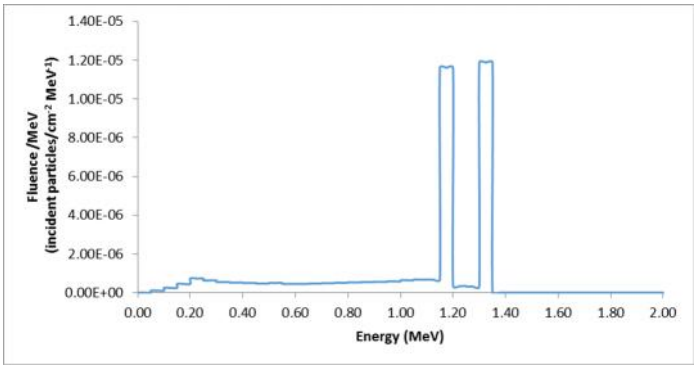

Figure 7: The Central Axis Energy Spectral Distribution for the Cobalt-60 Beam Phase Space showing the Prominent 1.173 MeV and 1.332 MeV Gamma Photo-peaks.

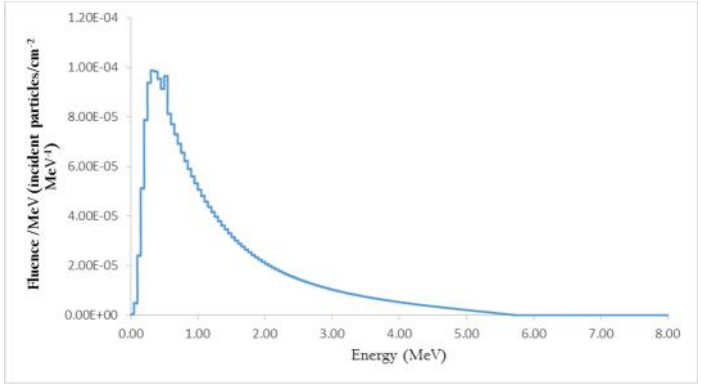

Figure 8: The Central-axis Energy Spectral Distribution for 6 MV Beam Phase Space showing Photon Particle Distribution at Low Energies

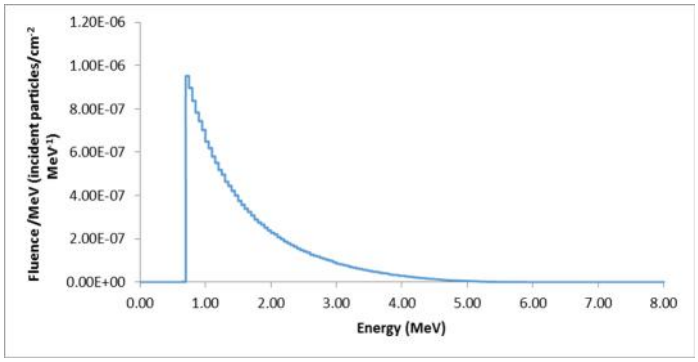

Figure 9: The Central-Axis Energy Spectral Distribution for 6 MV Beam Phase Space Showing Electron Particle Distributions at Low Energies

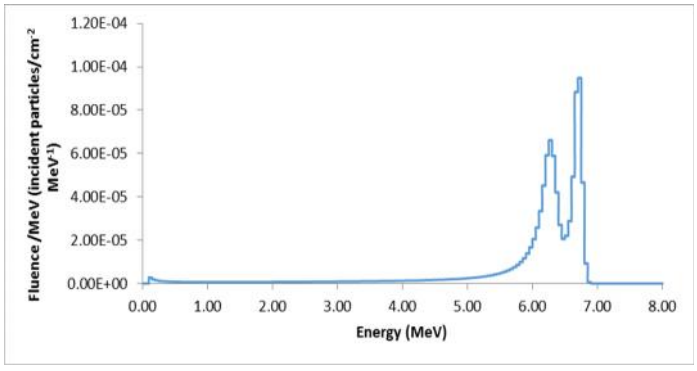

Figure 10: The Central-Axis Energy Spectral Distribution for 6 MeV Electron Beam Phase Space showing the Two (2) Prominent Electron Peaks.

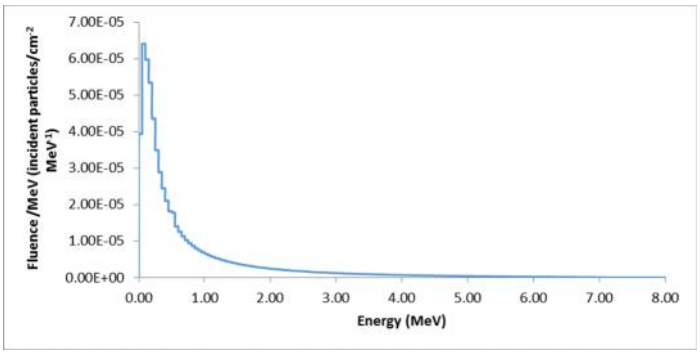

Figure 11: The Central-Axis Energy Spectral Distribution for 6 MeV Beam Phase Space showing Photon Particle Distribution at Low Energies

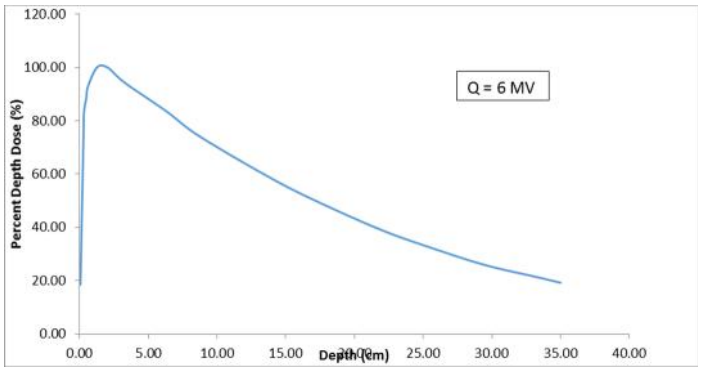

Figure 14: The Percent Depth Dose Profile in the Semi-Flex IC of a 6MV Beam from Monte Carlo Calculation at 10 x10 cm^2 Treatment Field and 100 cm SSD

it dose at the surface, the 6 MV X-ray beam deposits about 15 % of its dose at the surface and the 6 MeV electron deposits at the surface around 80 % of its

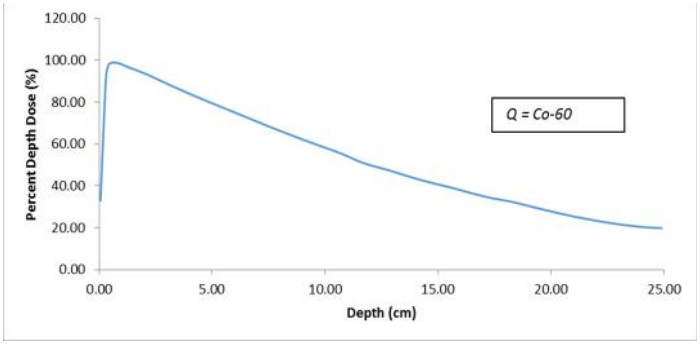

Figure 12: The Percent Depth Dose Profile in the Farmer IC of a Co-60 Beam from Monte Carlo Calculation at 10 x10 cm^2 Treatment Field and 100 cm SSD

absorbed dose and its maximum dose at a depth of around 1.6 cm.

It was also observed that the fall off regions of the Co-60 and 6 MV beams differ in height up to about depths of 10 cm. The higher fall off curve of the 6 MV was mainly attributed to the fact that the 6 MV photon beam attenuate less rapidly, create sec-

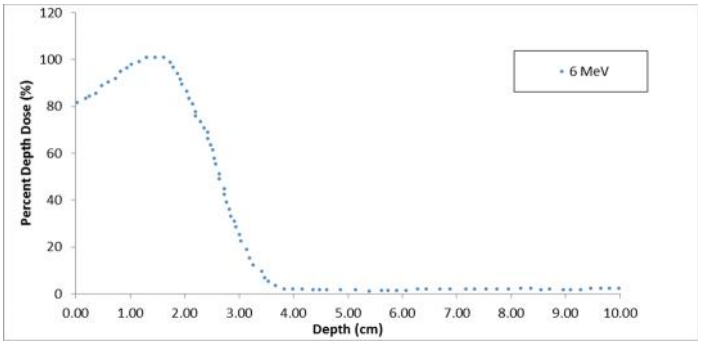

Figure 15: The Percent Depth Dose Profile of a 6 MeV Beam from Monte Carlo Calculation at 10 x10 cm^2 Treatment Field and 100 cm SSD of the Advanced Markus PTW 34045

ondary electrons that are more energetic to cause more ionization and thus more dose as the depth increases. Co-60 on the other hand attenuate more rapidly creating less energetic secondary electrons and

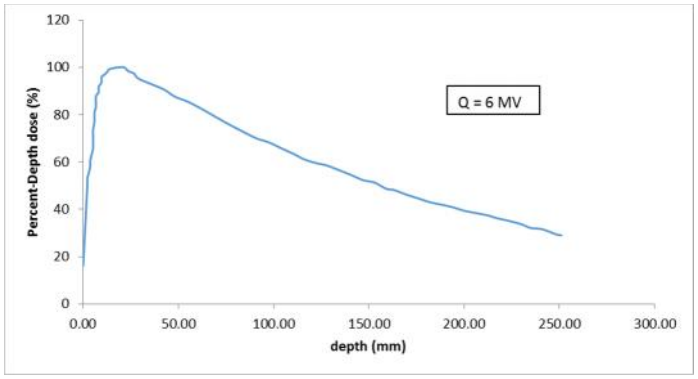

Figure 13: The Percent Depth Dose Profile of a 6 MV Beam for the Farmer IC from Monte Carlo Calculation at 10 x10 cm^2 Treatment Field and 100 cm SSD

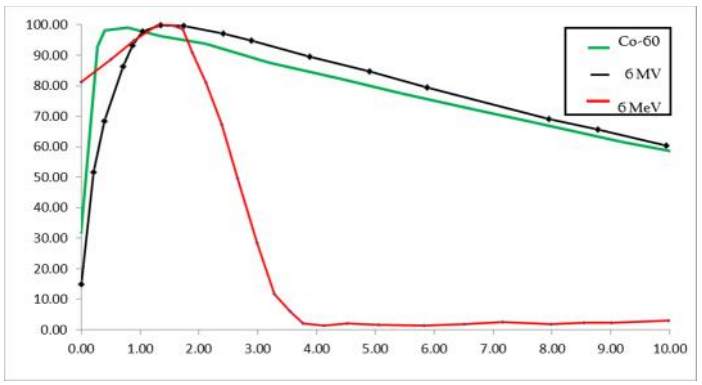

Figure 16: The Percent Depth-Dose Profile of the Co-60, 6 MeV and 6 MV Beam Qualities from Monte Carlo Calculation

Table 3: Comparison of Beam Quality Correction factors for the PTW 30013, PTW 31010 and PTW 34045 Ionization

Farmer Reference Ion Chamber											
PTW FARMER REFERENCE											
ENERGY E_0 (MeV)	$PDD_{20,10}$	$TPR_{20,10}$	*a*	b	C	d	K_Q (EXPT.) Aroh [15]	K_Q (M.C.) Sim.	K_Q (P_Q)	K_Q Wulff and Zink [7]	K_Q (PTW.) [11]
6.0000	0.5735	0.6666	2.2500	0.9798	1.0200	1.0761	0.991	0.992	0.993	0.9404	0.992
Semi-Flex Ion Chamber											
PTW 31010 SEMI-FLEX											
ENER-GY E_0 (MV)	***$PDD_{20,10}$***	***$TPR_{20,10}$***	**a**	**b**	**c**	**d**	***k_Q* (Expt.) Aroh [15]**	***k_Q* (M. C.) Sim.**	***k_Q* (P_Q)**	***k_Q* Wulff and Zink [7]**	
6.0000	0.6087	0.7112	1.733	2.772	1.516	1.285	0.995	0.986	0.994	0.985	
Advanced Markus Ion Chamber											
PTW 34045 ADVANCED MARKUS											
ENERGY E_0 (MeV)	**z_{ref}(cm)**	**Z_{ref}(eff.) (cm)**	***$R_{50,ion}$***	***R_{50}***	**$(P_{cav})_Q$**	**$(P_{wall})_Q$**	**$(_{sw,air})_Q$**	**$K_{q,E}$ (EXPT.) Aroh [15]**	**$K_{q,E}$ (M.C.) Sim.**	**$K_{q,E}$ PTW. [11]**	
6.0000	1.2500	1.1250	2.2400	2.2500	0.9798	1.0200	1.0761	0.9470	0.9404	0.9401	

so they get absorb within depths so quickly without interacting with more electrons around thereby causing ionization.

The 6 MeV electron beam, as shown in the beam profile in Figure 3.10, builds up its absorbed dose from about 80% of maximum at the surface depth to a maximum absorbed dose at around 1.7 cm from the surface of the phantom and then falls off far more rapidly into the Bremsstrahlung region (3.5 cm and above)

The 6 MeV beam profile was observed to have a practical range around 3.4 cm and a Bremsstrahlung tail from 3.4 cm into more depth within the phantom. The Bremsstrahlung tail was mainly because of photon contaminations since it was expected that the electrons would have lost their energies within the practical range. The build-up region of the electron beam was large due to the accumulation of knock-on electrons, which creates more electrons and rapidly comes to rest within the knock-on electron range, mostly at the point of more electron creation.

Table 4: Absorbed Dose-to-Water Calculated From Monte Carlo Simulation

Absorbed Dose –to-water for the Cylindrical Chambers					
Ion Chamber Model	***$D_{air,6\ MV}(z_{ref})$*** *(Gy/History) x 10^{-13}*	***$D_{w,6\ MV}(z_{ref})$*** *(Gy/History) x 10^{-13}*	***$D_{air,Co\text{-}60}(z_{ref})$*** *(Gy/History) x 10^{-13}*	***$D_{w,Co\text{-}60}(z_{ref})$*** *(Gy/History) x 10^{-13}*	***k_Q (M.C. Calculations)***
PTW 30013 Farmer	0.4073	0.5148	0.1817	0.2313	0.992
PTW 31010 Semi-Flex	0.4394	0.551	0.2058	0.2621	0.986
Absorbed Dose –to-water for the Plane-Parallel Chamber					
Ion Chamber Model	**$D_{air,6\ MeV}(z_{ref})$** (Gy/History) x 10^{-13}	**$D_{w,6\ MeV}(z_{ref})$** (Gy/History) x 10^{-13}	**$D_{air,Co\text{-}60}(z_{ref})$** (Gy/History) x 10^{-13}	**$D_{w,Co\text{-}60}(z_{ref})$** (Gy/History) x 10^{-13}	***k_Q (M.C. Calculations)***
PTW 34045 Advanced Markus	0.5153	0.5514	0.2292	0.2621	0.940

3.2.2 Comparisons of Depth-Dose from Beam Profiles

The graphs in Figure 13 show the different percent depth dose curves as a function of central-axis depth for the Co-60, 6 MV and 6 MeV beams. the sharp fall-off of the percent depth dose of the 6 MeV electron beam was its characteristics of dissipating all its energy out within surface depths compared with the 6 MV. Also the Co-60 beam and the 6 MV beam fall off slowly from their peaks and this make them distribute their energies over wider area at different depths.

All the observations above summarize the justification for the choice of Co-60 gamma and photon beams for deep treatments when compared to the electron beams since much of the absorbed dose in photon beams tend to accumulate at greater depths and fall of less rapidly at greater depths than electron beams, which accumulate at lesser depth and then fall of more rapidly within superficial depth. Electron beam with 6 MeV energy range was therefore only useful for superficial treatment.

3.2.3 Comparisons of M.C.-Calculated Results of kQ and Experimental Results of kQ

The calculations of the beam quality correction factors for the photon (MV) and electron (MeV) beams, as shown in Table 3, were obtained by the formalisms from IAEA codes of practice, and were compared with the empirical estimations as a function of the photon beam quality index (TPR20,10) [7] and with the perturbation approximations [9] used in other similar works.

Comparisons of kQ for the Co-60 and 6 MeV photon beams show that the PTW approach and the Monte Carlo simulation approach yields the best agreement with about 0.1 % difference from experimental values, while the perturbation corrections (PQ) approach yields a better agreement with about 0.2 % difference from experimental values. The empirical estimation approach had the least agreement with about 5 % difference from experimental values. Therefore, the Monte Carlo Ratio approach can be utilized for deriving the kQ the PTW 30013 chamber type using the beam-quality index.

The kQ value calculated for the PTW 31010 chamber, using Wulff and Zink empirical approach, was in agreement with the experimental values, with a deviation of about 1 %. So also, the perturbation method, which is IAEA gold standard, yielded the best approximation to the experimental value with about 0.1 % while the M.C. simulation method estimated a better agreement with a deviation of about 0.9 % than the values from experiment. It can be concluded from this results that the M.C. simulation method is a very good option of obtaining the kQ for the PTW 31010 Semi-Flex IC.

The kq,E values for the PTW 34045 Advanced Markus IC using the “Wulff-and-Zink” modified M.C. simulation method yielded a better approximation to the experimental kq,E by a deviation of about 0.697 %. The analog M.C. simulation method yielded kq,E value with a deviation of 0.739 %. Recent PTW Brochure estimated PTW 34045’s kq,E at 0.9401, which is only about 0.729 % different from the experimental values. The modified Monte Carlo Simulation method therefore is the best method of obtaining the kq,E for the PTW 34045 IC. In sum, the experimental calibration procedure practically take longer time than the theoretical approach, this makes validation of experimental kQs more effective.

3.2.4 Absorbed Dose –to-water Results

The absorbed dose-to-water outlined for each ion chamber model, as shown in Table 4, was derived from the depth-ionization curves and the expression in equation (3.9b) as prescribed in the methodology for each IC. The ratios between the dose to water to dose to air in the 6 MV beam and Co-60 beams for the two cylindrical ICs showed almost the same factor of depth ionization conversion. This is expected as a general rule in which photon beams have the stopping power ratios whose variations is negligible beyond the maximum depth (zmax) with less than about 0.1 %, unlike the stopping power ratios in the 6 MeV beams in which each dose at each depth have value of stopping power ratio wide in variation to the next dose-depth.

4.0 Conclusion and Recommendation

The BEAMnrc Monte Carlo package, BEAMDP program and DOSXYZ Grace plotting program and Microsoft (MS.) Excel have been used to obtain the simulated beam quality correction factor (k_{Qsim}, $k_{q,Esim}$) values for the respective user ICs. The beam-quality correction factors for the user ICs for the Elekta Precise LINAC beams could be derived from M.C. Simulations of the setup using the method described in the methodology as a function of the beam quality indexes. The results show that once the nature of the beam sources, accurate details of the Co-60 reference treatment head, User's LINAC treatment head, details of the essential components of the ionization chambers and Phantom, are well established, then it is possible to determine within accepted deviations, the beam-quality correction factors for the photon and electron beam calibrations.

References

[1] International Atomic Energy Agency, IAEA (2000). Absorbed dose determination in external beam radiotherapy: Technical Report Series Number 398. An International Code of Practice, Vienna: IAEA.

[2] American Association of Physicists in Medicine, AAPM. (1983). A Protocol for the determination of absorbed dose from high-energy photon and electron beams. Med. Phys., 10, 741-771.

[3] Andreo P. (1992). Absorbed dose beam quality factors for the dosimetry of high-energy photon beams Phys. Med. Biol., 37, 2189–2211.

[4] Medin J., Andreo P., Grusell E., Mattsson O., Montelius A. and Roos M. (1995) Ionization chamber dosimetry of proton beams using cylindrical and plane parallel chambers. Nw versus Nk ion chamber calibrations Phys. Med. Biol. 40 1161–76

[5] Niatel M.T., Perroche-Roux A.M. and Boutillon M., 1985, Two determinations of W for electrons in dry air, Phys. Med Biol. 30, 67-75.

[6] Sempau J, Andreo P, Aldana J, Mazurier J. and Salvat F., 2004, Electron beam quality correction factors 585 for plane-parallel ionization chambers: Monte Carlo calculations using the Penelope system. Phys. Med. Biol., 49, 4427–4444.

[7] Wulff J. and Zink K., 2008, Efficiency Improvements for Ion Chamber Calculations in High Energy Photon Beams. Med Phys. 35(4), 1328-36.

[8] González-Castaño DM, Hartmann GH, Sánchez-Doblado F, Gómez F, Kapsch RP, Pena J, Capote R, 2009, The determination of beam quality correction factors: Monte Carlo simulations and measurements. Phys Med Biol.54(15), 4723-41

[9] Zink K. and Wulff J., 2012, Beam Quality Corrections for Parallel-Plate Ion Chambers in Electron Reference Dosimetry. Phys Med Biol., 57(7), 1831-54.

[10] Amestoy W., 2015, Review of Medical Dosimetry - A Study Guide, First Edition, Springer, NY, 2015

[11] PTW-Freiburg, 2016, Ionizing Radiation Detectors including Codes of Practice. PTW, Freiburg, Germany. 76.

[12] Ma C. M. and Rogers D. W. O., 2013, BEAMDP User's Manual. NRCC Report PIRS-0509, NRCC, Ottawa.

[13] Burns D.T., Ding G.X. and Rogers D.W.O., 1996, R50 as a beam quality specifier for selecting stopping-power ratios and reference depths for electron dosimetry, Med. Phys. 23, 383–388.

[14] Capote R., Sánchez-Doblado F., Leal A., Lagares J. I., Arráns R. and Hartmann G. H., 2004, An EGSnrc Monte Carlo study of the micro-ionization chamber for reference dosimetry of narrow irregular IMRT beamlets. Med. Phys. 31, 2416–22.

[15] Aroh F., 2013, Determination of Beam Quality Correction Factors for Two Ionization Chambers of The LINAC Unit at UNTH (Master's Thesis) University of Nigeria, Enugu, Enugu State.